Available online at www.sciencedirect.com
SCIENCE DIRECT
ELSEVIER
Journal of Solid State Chemistry 177 (2004) 3021–3027
JOURNAL OF SOLID STATE CHEMISTRY
http://elsevier.com/locate/jssc

Structural, morphology and electrical studies of Sm-modified bismuth titanate thin films on Si (100)

W.L. Liu,[a,b,c,*] H.R. Xia,[a,b] H. Han,[d] and X.Q. Wang[b]

[a] School of Physics and Microelectronics, Shandong University, Jinan 250100, People's Republic of China
[b] National Laboratory of Crystal Materials, Shandong University, Jinan 250100, People's Republic of China
[c] Department of Material Science and Engineering, Shandong Institute of Light Industry, Jinan 250100, People's Republic of China
[d] Department of Physics and Astronomy, University of Alabama, Tuscaloosa, AL 35487-0324, USA

Received 6 March 2004; received in revised form 10 May 2004; accepted 11 May 2004

Available online 24 June 2004

Abstract

Samarium-substituted bismuth titanate ($Bi_{3.15}Sm_{0.85}Ti_3O_{12}$ (BSmT)) thin films have been grown on *n*-type Si (100) substrates by metalorganic decomposition and spin-coating technique. X-ray diffraction and scanning electron microscopy (SEM) analyses confirmed that the crystallinity of the films increases with increasing annealing temperature and the optimum temperature was found to be 700°C. The Raman measurement showed an increase in structural distortion due to the changed ionic radius and atomic mass of Sm ions. The current–voltage characteristics displayed good insulating properties for a film annealed at 700°C for 1 h. The capacitance–voltage characteristic hysteresis curves revealed that the ferroelectric property sufficiently controlled the silicon potential. The measurements of the dielectric constant and dissipation factor of BSmT as a function of frequency exhibited excellent dielectric properties.
© 2004 Elsevier Inc. All rights reserved.

PACS: 73.40; 77.55; 77.80; 81.20

Keywords: Crystal structure; Electrical properties; Ferroelectrics; Nanomaterials

1. Introduction

Bismuth titanate ($Bi_4Ti_3O_{12}$ (BTO)) is a member of the Aurivillius family of bismuth layer structure perovskites, which consists of three perovskite-like units, sandwiched between bismuth oxide layers along the *c*-axis as represented in Fig. 1, where *A*, *B*, and *C* denote the $(Bi_2Ti_3O_{10})^{2-}$ perovskite-like blocks, units of hypothetical perovskite structure, and $(Bi_2O_2)^{2+}$ sheets, respectively [1]. The Aurivillius phase is displacive ferroelectrics with a tetragonal *I*4/*mmm* structure, (*a, a, c*), above the Curie temperature T_c. It is common to define a doubled orthorhombic (pseudo-tetragonal) cell centered at Ti. This formally transforms the *I*4/*mmm* structure to an undistorted *Fmmm* parent structure $(a, b = a, c)$. The structure below T_c can be described by orthorhombic deviation from the undistorted *Fmmm* structure leading to $a \neq b$ [2].

As a typical perovskite layered structure ferroelectric materials, BTO has become a key candidate for memory storage capacitor, optical display and electro-optical devices owing to their promising ferroelectric and electro-optic properties [3–5]. Metal–ferroelectric–semiconductor (MFS) hetero-structure with BTO as a gate electrode material for ferroelectric field effect transistor (FFET) in a non-destructive readout mode has been demonstrated [6]. However, BTO films show fatigue and unexpectedly high leakage electric current, which have appeared as obstacles for further technological adoption [7].

For the specific applications, a small amount of impurity is important to tailor physical properties and microstructures of materials. The studies recently suggested that the Bi ions affect fatigue characteristics,

*Corresponding author. Department of Physics, Shandong University, Jinan 250100, PR China. Fax: +86-531856-5167.
E-mail address: liuwl@sdili.edu.cn (W.L. Liu).

0022-4596/$ - see front matter © 2004 Elsevier Inc. All rights reserved.
doi:10.1016/j.jssc.2004.05.016

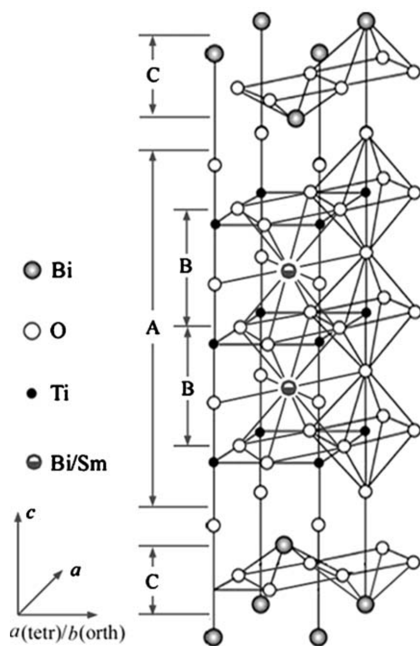

Fig. 1. Crystal structure of the BSmT.

and the failure characteristics of BTO could be improved if some Bi ions were substituted near the Ti–O octahedron layers with the lanthanide ions as illustrated in Fig. 1 [8,9]. The BTO doped with donors reduced the electrical conductivity and enhanced ferroelectric properties [10].

Thin films of BTO have already been prepared by RF sputtering [4], metalorganic chemical vapor deposition [11], pulsed laser deposition [6], and electron cyclotron resonance plasma sputtering [12], etc. Among the various techniques available for the fabrication of BTO thin films, metalorganic decomposition (MOD) method employed in this study offers the advantages of precise control of composition and homogeneity along with the ability to coat a large film on a complex substrate. Besides, as a ferroelectric material, $Bi_{3.15}Sm_{0.85}Ti_3O_{12}$ showed large remnant polarization, superior fatigue resistance and excellent charge-retention characteristics [9]. In view of these, the main purpose of the present study was to develop $Bi_{3.15}Sm_{0.85}Ti_3O_{12}$ (BSmT) thin films on *n*-type Si (100) substrates by MOD method and analyze the electrical properties for a MFS capacitor.

2. Experimental

The precursor for BSmT was prepared by first dissolving appropriate amount of bismuth nitrate and samarium nitrate into glacial acetic acid at room temperature. The solution was diluted with 2-methoxyethanol to adjust the viscosity and surface tension. Stoichiometric amount of titanium butoxide was slowly added to the mixed precursor. The 4% excess bismuth nitrate was used to compensate the loss of bismuth that was induced during the thermal annealing of amorphous films. In order to keep the precursor solution stable, it is necessary to add acetylacetone into the solution. Dust and impurities were removed by filtering through 0.2 μm syringe filters. Clear yellowish precursor solution was obtained.

BSmT films were fabricated onto the *n*-type Si (100) substrates by spin coating/heating cycle. The wet films were heated at 400°C in air for 20 min to remove residual organic. The resultant films were annealed at various temperatures ranging between 500°C and 800°C for 1 h.

As-annealed films were specular, crack-free, dense, and adhered well on the substrates used. The films were first examined by electron probe microanalysis to determine the composition and the obtained film compositions were in agreement with the nominal ones. The film thickness, as measured using a Dektak II stepmeter, was approximately 500 nm. The BSmT films were analyzed by X-ray diffraction (XRD) using a Rigaku D/MAX-γA X-ray diffractometer. The surface morphology of the films was analyzed by scanning electron microscopy (SEM). The Raman measurements were performed in the backscattering geometry using a Ventuno21 NRS-1000DT instrument at room temperature. The current–voltage (*I–V*) measurements were conducted using a pA meter/DC voltage source (HP 4140B). The capacitance–voltage (*C–V*) characteristics and the dielectric properties were measured using a LF Impedance Analyzer (HP 4192A).

3. Results and discussion

3.1. Structure characterization of BSmT films

3.1.1. XRD study

Fig. 2 shows the X-ray diffraction patterns of the $Bi_{3.15}Sm_{0.85}Ti_3O_{12}$ film prepared on Si (100) and annealed at various indicated temperatures for 1 h. XRD pattern of BTO films heat-treated at 400°C and 500°C confirmed the amorphous nature. This amorphous behavior remains unaltered up to an annealing temperature of 600°C. As the annealing temperature was increased, the peaks in the XRD pattern became sharper and the full-width at half-maximum (FWHM) decreased indicating better crystallinity and an increase in grain size with increasing annealing temperature. At 700°C, sharp and numerous peaks can be observed, indicating that the BSmT films crystallized very well. The XRD patterns also revealed that the films annealed at 700°C and above were polycrystalline in nature with no evidence of preferential orientation or second phase. The crystal orientation was not observed in the XRD

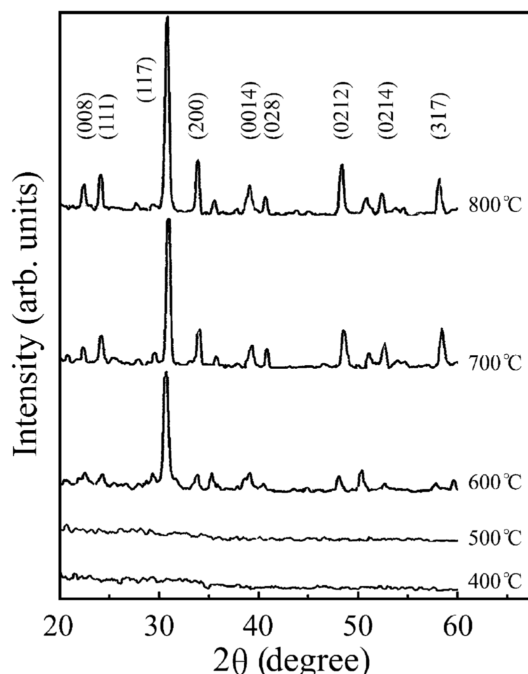

Fig. 2. X-ray diffraction patterns of BSmT films annealed at various indicated temperatures.

Table 1
Grain size as a function of annealing temperature

Annealing temperature (°C)	Grain size (nm)	
	XRD	SEM
600	37	70
700	56	120
800	68	160

pattern, which could be ascribed to the inevitable formation of SiO_2 layer during deposition. The unwanted silica layers with low permittivity at the ferroelectric/semiconductor interface, of which the thickness typically 2–7 nm, as a result, decrease the effective electric fields [13,14].

The average grain size t was estimated from the half-width of the X-ray diffraction peaks using Scherrer's equation

$$t = \frac{k\lambda}{\beta \cos \theta},$$

where θ is the diffraction angle, λ the average wavelength of X-ray, k the shape factor, and β is taken as half-maximum line breadth. The grain sizes of BSmT films annealed in the temperature range 600–800°C for 1 h were summarized in Table 1.

3.1.2. Surface morphology

The effects of the annealing temperature on the morphology of the films were analyzed by SEM. Fig. 3 shows the effects of annealing on the grain size of the films. The grain size increased with the increasing in annealing temperature. Larger grain size are expected with increasing temperature because of an increase in surface mobility, thus allowing the films to decrease their total energy by growing larger grains and decreasing their grain boundary area. The average grain size was in the range 70–160 nm for films annealed at the temperature of 600–800°C for 1 h. The grain sizes estimated from SEM observations in Table 1 were

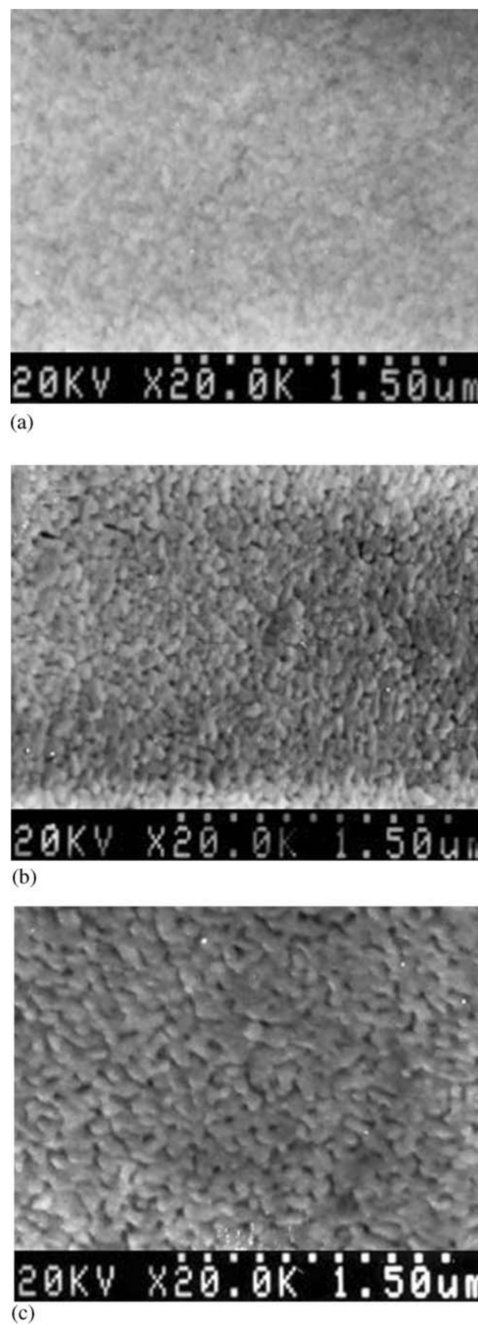

Fig. 3. SEM photographs of BSmT films annealed at (a) 600°C, (b) 700°C, and (c) 800°C.

different from those done by means of Schereer's equation. The Scherrer's equation assumes that all the crystallites are of the same size, but in an actual specimen, the size range and distribution affect β. Additionally, incoherent scattering from domains, distortions in the periodicity in the films, and micro-stress contribute to the line broadening and, hence, errors in the grain size estimation. Because the X-ray line broadening yields relative crystallite size, if absolute sizes are necessary then electron microscopy must be used to establish a basis for comparison.

3.1.3. Raman spectroscopy study

For films annealed at 700°C for 1 h, the lattice constants a, b, and c were calculated using (200), (117) and (111) peaks in the XRD pattern, and were found to be 5.452, 5.449, and 32.78 Å, respectively, suggesting that the films were crystallized in orthorhombic phase. The lattice constant values were slightly different from those of bulk BTO ($a = 5.4448, b = 5.410$, and $c = 32.83$ Å, ICCD file 35–0795). The slight difference between the BSmT and BTO films may be attributed to the structural variation with partial Sm substitution. The structural distortion of the material may result in different symmetries. Raman spectra from such regions should reveal the possible symmetry of the material.

If a tetragonal ($I4/mmm$) symmetry is assigned to the Aurivillius phases according to the calculated lattice parameters by the XRD pattern, the following Raman (R)- and infrared (IR)-active optical phonon modes in BTO at zero wavevector are [15]:

$$\Gamma_{\text{vib}} = 6A_{1g}(\text{R}) + 2B_{1g}(\text{R}) + 8E_g(\text{R}) + 9A_{2u}(\text{IR}) + 2B_{2u}(\text{IR}) + 11E_u(\text{IR}).$$

It is clear that theoretically observable Raman peaks, caused by the symmetric vibrations (g), are not more than 16 in number. The samples in the present work are polycrystalline films as was shown by the XRD pattern. It is, therefore, expected that the present Raman spectra for the thin films correspond to the powder spectra. We whereupon have also done Raman measurements on the BTO nanoparticle. Our Raman data on the BTO powder agreed with the published results, even though it is not quite exact for the mode counting in polycrystalline material, especially in thin films, due to possible symmetry breaking, low peak intensity and overlap of vibration modes [16].

The peaks at 301 and 520 cm^{-1} in the thin film spectra resulted from the vibration modes of the silicon substrate as marked in the figure. Compared to these of bulk crystal, Raman modes at 849, 614, 564, 320 and 350 cm^{-1} could be assigned as the A_{1g} and B_{1g} modes, respectively; the 537, 268, and 226 cm^{-1} modes could be assigned as $B_{2g} + B_{3g}$ modes originating from the lifting of E_g degeneracy.

In accordance with Raman data of $Bi_4Ti_3O_{12}$, $BaTiO_3$, and $PbTiO_3$ [15–17], a shorter bond length of Ti–O than that of Bi–O, suggests that the Raman phonon modes of the corresponding higher wavenumbers, such as the modes at 614 and 849 cm^{-1}, originated mainly from the vibrations of atoms inside the TiO_6 octahedra. The peak at 849 cm^{-1} was attributed to the symmetric Ti–O stretching vibration, while the 614 cm^{-1} to asymmetric one; the 268 and 226 cm^{-1} modes were ascribed to the O–Ti–O bending vibration. Although the mode at 226 cm^{-1} is Raman inactive according to the O_h symmetry of TiO_6, it is often observed because of the distortion of octahedron. The mode at 320 was from a combination of the stretching and bending vibrations. The two modes at 537 and 564 corresponded to the opposing excursions of the external apical oxygen atoms of the TiO_6 octahedra. The TiO_6 octahedra showed considerable distortion at room temperature so that some phonon modes, e.g. at 320, 537, 614, and 849 cm^{-1}, appeared wide and weak. The increase on distortion of TiO_6 octahedra with Sm-substitution of Bi led to a relatively large wavenumber change by careful comparison and analysis of BTO powder and BSmT films annealed at 700°C for 1 h showed that these Raman peaks, e.g. at 614 and 849 cm^{-1} were found to increase to 620 and 854 cm^{-1}, respectively (Fig. 4). The shifts could be attribute to the changed ionic radius and atomic mass of Sm ions, as Bi ions do not participate in the vibrations.

The Raman modes of the corresponding lower wavenumbers, such as the modes at 118 cm^{-1}, originated mainly from bending and torsional modes of the titanium and bismuth polyhedra, those aspects of the structure that are most involved with ferroelectric ordering. The sharp mode at 118 cm^{-1} shifted to 126 cm^{-1} due to the substitution of a lighter Sm atom at Bi site, as depicted in Fig. 1. The amendment of ferroelectricity is therefore expected due to the variation of electronic structure in nature with Sm-modification of Bi. Besides, an increase in peak intensity with increasing temperature indicating better crystallinity is coincident with the XRD and SEM results. The presence of any additional symmetry that might have originated from the structural distortions could not be established. Further study is necessary to clarify the microstructure change due to Sm substitution.

3.2. Electrical properties of BSmT thin films

Some electrical properties of BSmT films were studied. Gold dots of 0.8 mm diameter on the BSmT film as top electrodes and Au film was sputtered on the back of the silicon substrate as a bottom electrode to form a metal/ferroelectric/semiconductor/metal (MFSM) configuration.

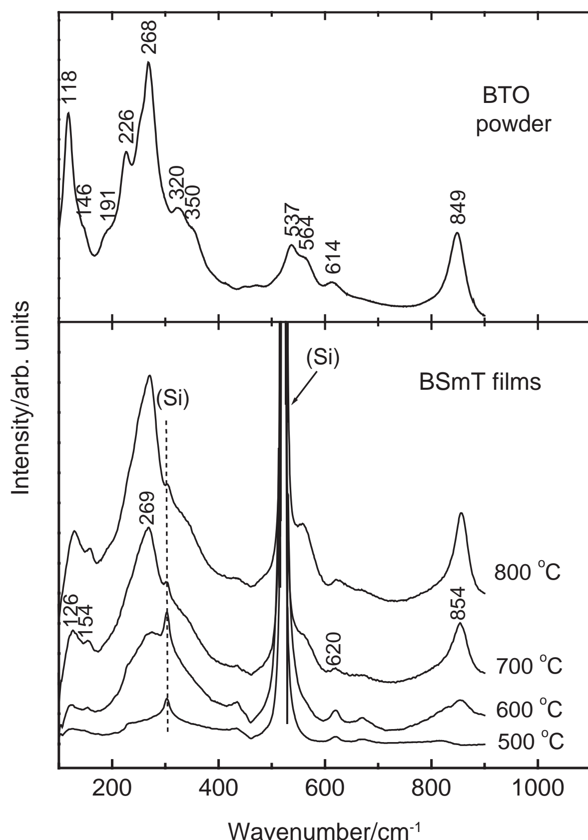

Fig. 4. Raman spectra for BTO powder and BSmT films on Si substrate.

3.2.1. I–V characteristics

The *I–V* characteristics were measured on a 500-nm-thick BSmT thin film in the MFSM capacitor. Fig. 5 is a typical log(*I*) versus log(*V*) curve for BSmT thin film annealed at 700°C for 1 h. The BSmT film exhibited a resistivity in the range of 10^8–10^{11} Ω cm when a DC bias of 0–5 V applied to the capacitor. In this range of resistivities the electrical conduction is proposed to be space-charge-limited as discussed later [18]. The leakage current significantly increased for voltages more than 5 V. The data above indicated that BSmT thin films directly deposited on the Si (100) substrates by MOD technique had good insulating property and resistance to breakdown.

At low voltages (below 2 V), current I was linearly dependent on voltage V, i.e., the *I–V* curve exhibited ohmic behavior. According to space-charge-limited-current (SCLC) theory, this Ohmic mode occurs in insulating film as long as the film is quasineutral, that is, as long as the bulk generated current in the film exceeds the current due to injected free carriers from the electrode. The current–voltage dependence in the Ohmic region is given by [19]

$$I = n_0 q \mu A V / d,$$

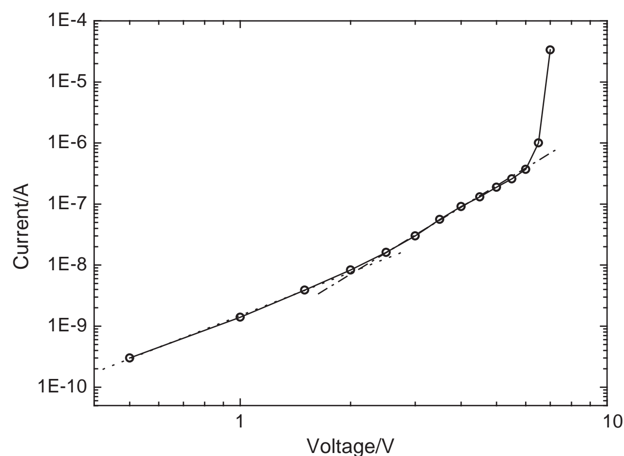

Fig. 5. Typical log(*I*) vs log(*V*) curves for a BSmT thin film annealed at 700°C for 1 h.

where n_0 is the concentration of charge carriers, q the electronic charge, μ the mobility, A the area of the electrodes, and d the film thickness. At higher fields (above 2 V), the nonlinear *I–V* relationship could be observed. According to SCLC theory, as applied voltage is increased, the injection of charge carriers in the bulk of the film takes place. For stronger injection, the insulator traps fill up and a space charge appears. The space-charge effects are observed when the injected free carrier density exceeds the volume generated free carrier density. A square law region appeared above 2 V indicating onset of the space-charge-limited conduction. In this square law region the current is given by [19]

$$I = 9\varepsilon\mu\theta A V / 8d^3,$$

where ε is the absolute dielectric constant of the film, and θ the ratio of the free electron density and the density of filled trapping sites. As the applied voltage is increased further, very strong injection of charge carriers takes place and causes an increase in the density of filled trapping sites. If sufficient charge is injected into the insulator, all the traps will become filled. Further injected charge then exists as free charge in the conduction band and contributes to the current. Higher power law region could be observed in the *I–V* characteristics as applied voltage higher than 6 V. According to the SCLC theory, the concentration of traps is given by [19]

$$N_t = \varepsilon_0 \varepsilon_r V_{TFL} / q d^2,$$

where N_t is the concentration of traps, ε_r the dielectric constant of the film, ε_0 the permittivity of free space, and V_{TFL} the trap-filled voltage limit. The discussions above indicated that BSmT films showed excellent insulating property in the low voltage range. It is of great importance for use in large-scale integrated circuit processes.

3.2.2. C–V characteristics

Fig. 6 is the C–V curves measured at 100 KHz for the MFSM structured BSmT films with the thickness of 500 nm at the sweep voltages of 3 and 5 V. Both of the C–V characteristics exhibited clear regions of accumulation, depletion and inversion. The counterclockwise C–V hysteresis indicated by the arrows are attributable to ferroelectric polarization, which is the desired mode for memory operation [20]. When the bias voltages swept from -3 to 3 V and back to -3 V, the capacitances in the accumulation region were still not coincide, indicating that the memory window was unsaturated. At sweep voltage amplitude was ± 5 V, the accumulation and depletion of the C–V curve were coincided, and the memory window of the loop was around 3.6 V. Not only did the capacitance values saturate to the maximum and minimum values in both the accumulation and the inversion regions, respectively, but there were no features such as either humps or valleys detectable in the C–V curves. The featureless C–V characteristics suggested that neither a large leakage current nor a significant carrier injection occurred. Besides, the memory window increased symmetrically with the sweep voltage, which meant that the memory window increased due to the ferroelectric polarization without charge injection. Furthermore, the hysteresis loops were relatively "square" indicating that the memory retention was very stable. The C–V curves showed that the capacitance varied from the depletion state to the accumulation state, and the direction of the hysteresis loop was consistent with ferroelectric polarization switching.

The consistent results of C–V and I–V measurement suggested that Sm-modification could improve the ferroelectric properties of metal/BSmT/Si structured materials, increase the memory window of the C–V loop and amend the insulating properties of thin films to satisfy the application in FFET device.

The fixed charge within the BSmT films should be low if the films are to be used for an insulating gate. According to the C–V curve, the fixed charge density (N_{fc}) can be calculated from the following formula:

$$N_{fc} = -C_{max} \times (V_{FB} - \Phi_{MS})/(qA).$$

The maximum capacitance (C_{max}) measured corresponded approximately to the capacitance of the ferroelectric. V_{FB}: flatband voltage; Φ_{MS}: effect function remainder between metal electrode and semiconductor substrate; q: electronic charge; A: electrode area. The resistivity of n-type Si is 5–7 Ω cm, and the doped concentration is $4 \times 10^{14}\,\text{cm}^{-3}$. The values of N_{fc} was found to be about $5 \times 10^{11}\,\text{cm}^{-2}$.

The fast surface-state parameters in a BSmT/Si MFS capacitor have also been calculated. The measured conductance (G) can be utilized to determine the surface-state density (N_{ss}) because it directly relates to surface states [21]

$$G/\omega = C_s\omega\tau/(1+\omega^2\tau^2),$$

$$N_{ss} = C_s/qA,$$

where ω is the angular frequency, C_s the surface-state capacitance, τ the time constant, q the electronic charge, and A the electrode area. When the conductance goes through a maximum, $\omega\tau = 1$, which $C_s = 2G/\omega$, then the surface-state density N_{ss} can be obtained by using the following formula:

$$N_{ss} = 2G_{max}/(\omega qA).$$

The results obtained showed that the surface-state density was around $1 \times 10^{12}\,\text{cm}^{-2}\,\text{eV}^{-1}$.

The values of N_{fc} and N_{ss} of the BSmT film are considered to be adequate for a FFET operation.

3.2.3. Dielectric characteristics

Fig. 7 shows the dielectric constant and dissipation factor measured at room temperature as a function of frequency in the range from 1 KHz to 1 MHz. The dielectric constant of the BSmT capacitor slightly

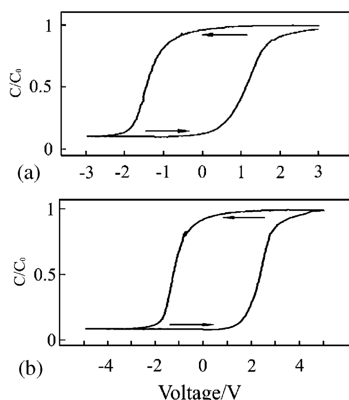

Fig. 6. C–V characteristics of BSmT films, where $C_0 = 1620$ pF.

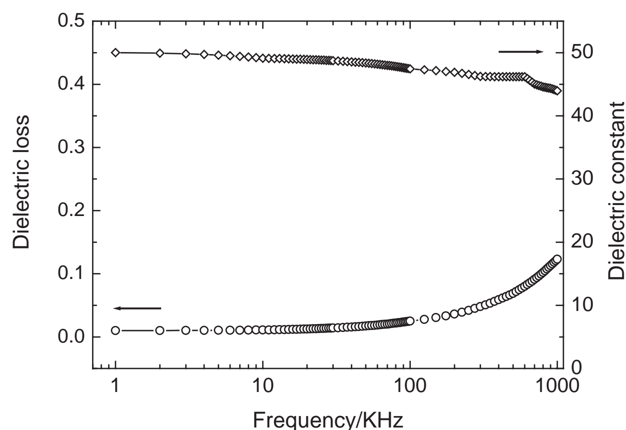

Fig. 7. Dielectric constant and dissipation factor (loss) for the Au/BSmT/Si/Au films as a function of frequency.

decreased with increasing frequency, but it was much more stable than that of BTO [22]. There were no sudden changes of the dielectric constant and the dissipation factor within the frequency range up to 1 MHz, indicating the compositional homogeneity and thickness uniformity of the film. Besides, the dissipation factor at 1 MHz was measured to be 0.14, which is much lower than those of BTO and BLT films [22,23].

4. Conclusions

$Bi_{3.15}Sm_{0.85}Ti_3O_{12}$ thin films have been successfully produced on *n*-type Si (100) substrates by MOD technique. BSmT films began to crystallize at an annealing temperature of 600°C. BSmT films annealed at 700°C for 1 h had good crystallization. The shift of some modes to higher wavenumber implied an increase in structural distortion due to the changed ionic radius and atomic mass of Sm ions. Room temperature resistivity of $10^8\,\Omega\,cm$ and leakage current of less than 10^{-8} A were obtained for a 500-nm-thick film, establishing good insulating behavior. The *I–V* characteristics showed ohmic conductivity in the lower voltage range and space-charge-limited conductivity at higher field. The dielectric properties and the *C–V* characteristic hysteresis curves, as well as the calculated results of N_{fc} and N_{ss}, showed that BSmT thin films obtained by MOD method have promising applications as FFET memories.

Acknowledgments

The authors thank Dr. Tim Williams (Jasco International Co. Ltd.) for technical help. This work was supported by the National Natural Science Foundation of China (10274043), Shandong Provincial Natural Science Foundation and Project for Key Task.

References

[1] R.E. Newnham, R.W. Wolfe, J.F. Dorrian, Mater. Res. Bull. 6 (1971) 1029.
[2] R.L. Withers, J.G. Thompson, A.D. Rae, J. Solid State Chem. 94 (1991) 404.
[3] S.E. Cummins, L.E. Cross, Appl. Phys. Lett. 10 (1967) 14.
[4] K. Suibuchi, Y. Kurogi, N. Endo, J. Appl. Phys. 46 (1975) 2877.
[5] W. Jo, H.-J. Cho, T.W. Noh, B.I. Kim, D.-Y. Kim, Z.G. Khim, S.-I. Kwun, Appl. Phys. Lett. 63 (1993) 2198.
[6] H. Buhey, S. Sinharoy, W.H. Kasner, M.H. Francombe, Appl. Phys. Lett. 58 (1991) 1470.
[7] H. Nagata, N. Chikushi, T. Takenaka, Jpn. J. Appl. Phys. Lett. 38 (1999) 5497.
[8] B.H. Park, B.S. Kang, S.D. Bu, T.W. Noh, J. Lee, W. Jo, Nature (London) 401 (1999) 682.
[9] U. Chon, K.B. Kim, H.M. Jang, G.C. Yi, Appl. Phys. Lett. 79 (2001) 3137.
[10] Y. Noguchi, M. Miyayama, Appl. Phys. Lett. 78 (2001) 1903.
[11] T. Li, Y. Zhu, S.B. Desu, C.H. Peng, M. Nagata, Appl. Phys. Lett. 68 (1996) 616.
[12] H. Masumoto, T. Goto, Y. Masuda, A. Baba, T. Hirai, Appl. Phys. Lett. 58 (1991) 243.
[13] S.G. Ghong, E. Goo, R. Ramesh, R. Haakennaaser, D.K. Fork, Appl. Phys. Lett. 64 (1994) 3407.
[14] H.N. Lee, Y.T. Kim, Y.K. Park, Appl. Phys. Lett. 74 (1999) 3887.
[15] P.R. Graves, G. Hua, S. Myhra, J.G. Thompson, J. Solid State Chem. 114 (1995) 112.
[16] H. Idink, V. Srikanth, W.B. White, E.C. Subbarao, J. Appl. Phys. 76 (1994) 1819.
[17] P.S. Dobal, R.S. Katiyar, J. Raman Spectrosc. 33 (2002) 405.
[18] A.E. Rakhshani, J. Appl. Phys. 69 (1991) 2365.
[19] J.G. Simmons, Handbook of Thin Film Technology, McGraw-Hill, New York, 1970.
[20] N. Maffei, S.B. Krupanidhi, J. Appl. Phys. 72 (1992) 3617.
[21] E.H. Nicollian, A. Goetzberger, Appl. Phys. Lett. 7 (1965) 216.
[22] X.M. Wu, H. Wang, Z. Wang, S.X. Shang, M. Wang, J. Funct. Mater. Suppl. (2000) 67 (in Chinese).
[23] Y. Hou, Ph.D. dissertation, Shandong University, China, 2002.